Journal of Asian Earth Sciences 156 (2018) 316–330

Contents lists available at ScienceDirect

Journal of Asian Earth Sciences

journal homepage: www.elsevier.com/locate/jseaes

Full length article

Moho depth variations over the Maldive Ridge and adjoining Arabian and Central Indian Basins, Western Indian Ocean, from three dimensional inversion of gravity anomalies

Priyesh Kunnummal[a], S.P. Anand[a,*], C. Haritha[b], P. Rama Rao[c]

[a] Indian Institute of Geomagnetism, Navi Mumbai, Maharashtra 410218, India
[b] Cochin University of Science & Technology, Cochin, Kerala, India
[c] Andhra University, Vishakapatanam, Andhra Pradesh 530 003, India

ARTICLE INFO

Keywords:
Chagos-Laccadive Ridge
Maldive Ridge
Free air gravity anomaly
Moho undulations
Crustal thickness
Gravity inversion

ABSTRACT

Analysis of high resolution satellite derived free air gravity data has been undertaken in the Greater Maldive Ridge (GMR) (Maldive Ridge, Deep Sea Channel, northern limit of Chagos Bank) segment of the Chagos Laccadive Ridge and the adjoining Arabian and Central Indian Basins. A Complete Bouguer Anomaly (CBA) map was generated from the Indian Ocean Geoidal Low removed Free Air Gravity (hereinafter referred to as "FAG-IOGL") data by incorporating Bullard A, B and C corrections. Using the Parker method, Moho topography was initially computed by inverting the CBA data. From the CBA the Mantle Residual Gravity Anomalies (MRGA) were computed by incorporating gravity effects of sediments and lithospheric temperature and pressure induced anomalies. Further, the MRGA was inverted to get Moho undulations from which the crustal thickness was also estimated. It was found that incorporating the lithospheric thermal and pressure anomaly correction has provided substantial improvement in the computed Moho depths especially in the oceanic areas. But along the GMR, there was not much variation in the Moho thickness computed with and without the thermal and pressure gravity correction implying that the crustal thickness of the ridge does not depend on the oceanic isochrones used for the thermal corrections. The estimated Moho depths in the study area ranges from 7 km to 28 km and the crustal thickness from 2 km to 27 km. The Moho depths are shallower in regions closer to Central Indian Ridge in the Arabian Basin i.e., the region to the west of the GMR is thinner compared to the region in the east (Central Indian Basin). The thickest crust and the deepest Moho are found below the N-S trending GMR segment of the Chagos-Laccadive Ridge. Along the GMR the crustal thickness decreases from north to south with thickness of 27 km below the Maldives Ridge reducing to ~9 km at 3°S and further increasing towards Chagos Bank. Even though there are similarities in crustal thickness between Maldive Ridge and other regions like Mascarene Plateau which was recently interpreted as underlain by continental crust, much more geoscientific work including drilling has to be undertaken to finally confirm the exact nature of the ridge.

1. Introduction

Group of non-spreading, topographically elevated linear features on the seafloor formed either by volcanic eruption along a leaky transform fault or hotspot or through uplift and rifting associated with tectonic activities are termed aseismic ridges (Mukhopadhyay et al., 2008). These ridges will have very minimal to no seismic activity associated with them. Two such prominent aseismic ridges in the Indian Ocean are the Ninety East Ridge in the Eastern Indian Ocean and the Chagos-Laccadive Ridge in the Western Indian Ocean. The Chagos-Laccadive Ridge (CLR), is an approximately N-S trending prominent aseismic ridge stretched over 3000 km from about 10°S to 15°N. The CLR system consists of three segments; from the south these are respectively Chagos Bank, Maldive Ridge and Laccadive Plateau (Bhattacharya and Chaubey, 2001). These segments of the Chagos-Laccadive Ridge are separated by prominent E-W trending depressions. The islands of Chagos, the Maldives and Lakshadweep are above-water parts of the Chagos-Laccadive Ridge. Although the Chagos-Laccadive Ridge is an aseismic ridge, between 1965 and 1970 an unusual, isolated swarm of earthquakes occurred on the west side of the Great Chagos Bank. A number of theories have been postulated regarding the origin of the CLR (Bhattacharya and Chaubey, 2001); a zone of transition between oceanic crust in the west and continental crust in the east (Narain et al., 1968), a leaky transform fault (Fisher et al., 1971, Sclater and Fisher,

* Corresponding author.
E-mail address: aerospl@yahoo.co.uk (S.P. Anand).

https://doi.org/10.1016/j.jseaes.2017.12.012
Received 10 May 2017; Received in revised form 5 December 2017; Accepted 7 December 2017
Available online 09 December 2017

1974), a hot spot trace (Francis and Shor, 1966, Dietz and Holdon, 1970, Morgan, 1981), micro-continent etc. It was also proposed that different segments of the CLR have different genesis (Avraham and Bunce, 1977); Chagos Bank is composed of volcanic material associated with leaky transform fault, the Maldive Ridge is a microcontinent and the Laccadive Plateau is a continental fragment (Naini and Talwani, 1983) and intermingled with volcanic intrusives (Chaubey et al., 1998) which was once part of the Western Dharwar craton (Nair et al., 2013). Recently, analysis and dating of Zircons, from the basaltic beach sand samples (Torsvik et al., 2013) and trachytic rocks (Ashwal et al., 2017) of Mauritius Islands along with the crustal thickness estimation led to postulate that the Mauritius Islands and Mascarene Plateau overlie submerged, Precambrian micro-continent, coined, “Mauritia” (Torsvik et al., 2013) that was once a part of the ancient nucleus of Madagascar and southern India. The continental fragment of Mauritia included Saya de Malha, Chagos, Laccadive, Cargados-Carajos Bank, Nazreth etc. Thus, from the foregoing discussions it can be seen that several hypothesis has been postulated for the nature and evolution of the Chagos-Laccadive. A detailed understanding of the nature of the crust underlying the various aseismic ridges in the Indian Ocean is of paramount importance as some of these ridges are currently considered by several researchers as underlain by continental crust or continental slivers. Even though considerable amount of geophysical work has been carried out to understand the nature of crust underlying the Laccadive Plateau of the CLR, not much work has been undertaken in the region extending from Maldive Ridge to the Chagos Bank. As a first step to understanding the nature of the crust, in the present paper, an attempt has been made to estimate the Moho depth and crustal thickness variation in the Maldive Ridge and adjoining Arabian and Central Indian Basin using high resolution satellite derived Free Air gravity data. The crustal thickness and Moho depth, place first order constraints in understanding the tectonic and geochemical processes that have led to crustal formation and evolution. To accomplish this, Moho undulation and the crustal thickness of the Maldive Ridge and adjoining regions were computed by inversion of the gravity data incorporating lithospheric thermal and pressure gravity anomaly correction in addition to sediment gravity correction.

2. Morpho-tectonic elements and previous studies

The bathymetric map (V18.1, Smith and Sandwell, 1997) depicting major structural features in the region under study, derived from satellite altimetry having a resolution of one arc minute, is presented in Fig. 1. The study area is demarcated by white rectangle. A larger area is shown in Fig. 1 for better perspective of the morpho-tectonic elements of the study area and the adjoining regions. The study area comprises the Maldive Ridge, and the Deep Sea Channel between the Maldive Ridge and northern part of the Chagos Bank. For ease of discussion, in the present study, these two parts of the CLR is combined and termed as Greater Maldive Ridge (GMR). An archipelago of coral islands rests on each of the ridges. The region to the west of GMR is the young oceanic lithosphere of the Arabian Basin while the eastern side is part of the older Central Indian Basin. The Laccadive Plateau segment of the CLR is bounded by the offshore extension of Chapporo lineament in the north and Bhavani shear in the south (Nair et al., 2013) and was interpreted as a part of the Western Dharwar craton before rifting from India. Seismic reflection studies (Francis and Shor,1966) over the Maldive Ridge segment lying between 7°N and 1°S suggested presence of a thick sedimentary basin within the ridge. Three ODP wells (leg 115 sites 714, 715, 716, location shown in Fig. 1) were drilled in the northern part of the Maldive Ridge of which well 715 reached Early Eocene (57 Ma) basaltic basement around 210 m below seafloor (Backman et al., 1988). The basalts drilled from the Maldive Ridge (site 715) were sub-alkaline olivine basalts while that drilled from the Chagos Bank (713) were olivine tholeiite basalts showing affinity to Mid Oceanic Ridge Basalts. From the composition of the basalts it was inferred that basalts from Site 715 were erupted onto an isolated oceanic island that was distant from ocean ridges and has a mineralogy that is dominated by olivine as compared with the plagioclase-rich lavas of the other sites (713) (Fisk and Howard, 1990). Duncan and Hargraves (1990) also suggested that the lava solidified at sub-aerial depths at site 715 while at site 713 the lava poured out at greater depths. Location of the seismic refraction surveys carried out over CLR and adjoining areas (Francis and Shor, 1966) is superposed on Fig. 1. Refraction Station.1, in the region between Maldive Ridge and Laccadive Plateau (north of the present study area), 1.5 km thick layer of either chert or shallow water sandstone or lime stone was found to overlie a 5.00 km/s velocity layer followed by 10 km thick crust and Moho at depth of 17 km. Beneath stations 4 and 5, located in the Deep Sea Channel between Maldive Ridge and Chagos Bank, a 5 km thick layer with a velocity of 6.13 km/s overlies a 7.1 km/s crustal layer (Francis and Shor, 1966). Sea-floor spreading anomalies were not identified along the CLR (Avraham and Bunce, 1977) while well-defined spreading anomalies were identified in the Arabian Basin and southern part of the Central Indian Basin (McKenzie and Sclater, 1971). In the study area, the oldest spreading anomaly identified in the Central Indian Basin is A34 (Cande and Patriat, 2015) while that in the Arabian Basin is much younger.

Previous studies have aimed at postulating different evolutionary models for the origin of the Chagos-Laccadive Ridge. Studies prior to the eighties have suggested the Chagos-Laccadive Ridge and Mascarene Plateau evolved along a leaky transform fault (Fisher et al., 1971, McKenzie and Sclater, 1971), a volcanic feature as the Indian plate moved over the Reunion hotspot (Morgan, 1972; Dietz and Holden, 1970), a micro-continent (Krishnan, 1960; Davis, 1928), a volcanic feature associated with leaky transform fault or movement over a hotspot area (Avraham and Bunce, 1977), etc. Through the analysis of transfer function between free air gravity and bathymetry, Ashalatha et al. (1991) showed that the ridge is compensated locally with an Airy crustal thickness of 20 km. They have attributed the computed low elastic thickness to the volcanism of the ridge which took place near to spreading center. A synthesis of available data made Pushcharovsky (1996) to argue that the origin of the ridge cannot be associated either with transform fault or as a trace of the plate passage above the Reunion hot spot. Integrating the results from seismic refraction studies with the high amplitude magnetic anomalies a volcanic origin was assigned for the Maldive-Chagos section of the CLR while lack of appreciable magnetic anomalies over the Laccadive-Maldive stretch suggested a continental origin for this part of the ridge (Mukhopadhyay et al., 2008).

3. Data source and methodology

High-resolution satellite derived Free Air Gravity (FAG) data (V.24.1, Sandwell and Smith, 2009; Sandwell et al., 2014) generated from re-tracked Seasat, Geosat GM, TOPEX/POSEIDON, ERS-1/2, Cryosat-2 and Jason-1 altimeter data (ftp://topex.ucsd.edu/pub/global_grav_1min/) and bathymetry data (V.18.1, Smith and Sandwell, 1997) derived from satellite altimetry, each having a resolution of one arc minute is used in the present study for the regional data analysis. The basic approach by Smith and Sandwell (1997) is to filter the satellite gravity data over the 16- to 160-km wavelength band and downward continue the filtered gravity to the mean seafloor depth. The topography/gravity ratio was then regionally calibrated using the local topography at points constrained by soundings and adjust the transfer function for the effects of regionally varying sediment thickness. A good coherency was shown between ship-borne bathymetry and bathymetry by Smith and Sandwell (1997) for wavelengths > 100 km which suggests that the later bathymetry data set can be used for studies related to Moho undulations. As the current version (V.24.1) of the FAG data contain information down to very short wavelengths (< 20 km), this data set can be utilized for regional as well as detailed investigations. The region under study overlies the region occupied by

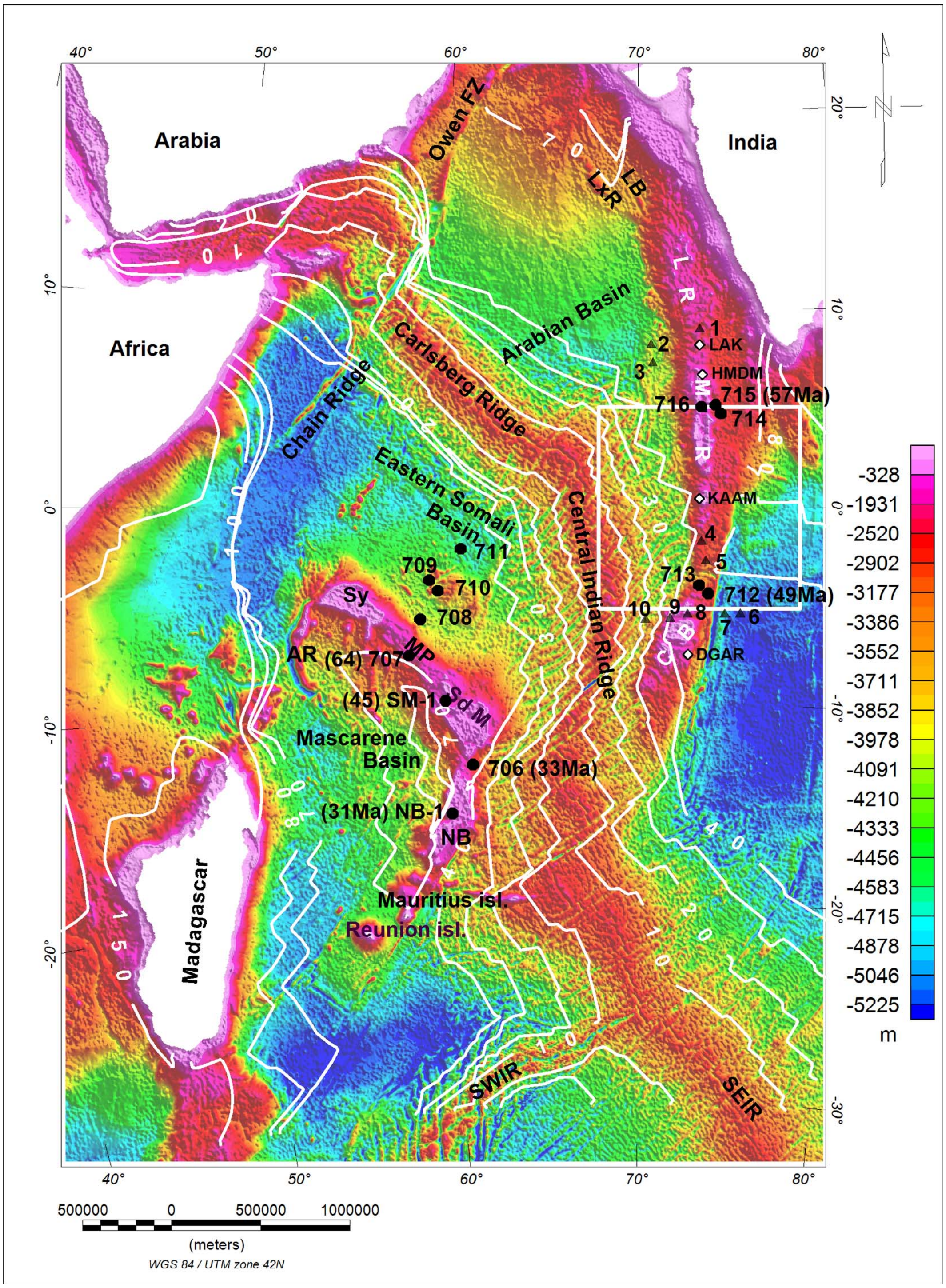

Fig. 1. Bathymetry map of the Western Indian Ocean generated from satellite altimetry (Smith and Sandwell, 1997) depicting major structural and tectonic features in the study region and adjoining areas. White rectangle demarcates the region under study. White solid lines represent contoured magnetic isochrones (Müller et al., 2008). The solid black triangles and circles respectively indicates seismic refraction stations (Francis and Shor, 1966) and the ODP well site (Backman et al., 1988) locations. **LB:** Laxmi Basin, **LxR:** Laxmi Ridge, **LR:** Laccadive Ridge, **MR:** Maldive Ridge, **CB:** Chagos Bank, **FZ:** Fracture Zone, **SWIR:** South West Indian Ridge, **SEIR:** South East Indian Ridge, **Sy:** Seychelles, **AR:** Amirante Ridge, **SdM:** Saya de Malha, **MP:** Mascarene Plateau, **NB:** Nazareth Bank. The white diamonds show the location of permanent broadband seismic stations used for receiver function studies (Fontaine et al., 2015).

the Indian Ocean Geoid Low (IOGL) (Kahle et al., 1978) which is characterized by long spatial wavelength anomalies whose origin is thought to lie in the mantle. As the present study is aimed at the crustal and upper mantle component (up to Moho), the long wavelength gravity anomalies originating from the deep mantle is removed from the Free-air anomaly. The long wavelength gravity effect of IOGL is calculated from geoid data (http://icgem.gfz-potsdam.de, Barthelmes and Köhler, 2016) using the spherical harmonic coefficient of EIGEN-6C4 (Förste et al., 2015) up to a degree and order of 50. A low pass filter corresponding to spherical harmonic degree 50 (~800 km) was used and the coefficients are rolled off between the degrees 30–70 in order to avoid the ringing effect arising due to sharp truncation at degree 50. The long wavelength gravity anomaly thus computed is removed from the FAG anomaly (V.24.1, Sandwell and Smith, 2009; Sandwell et al.,

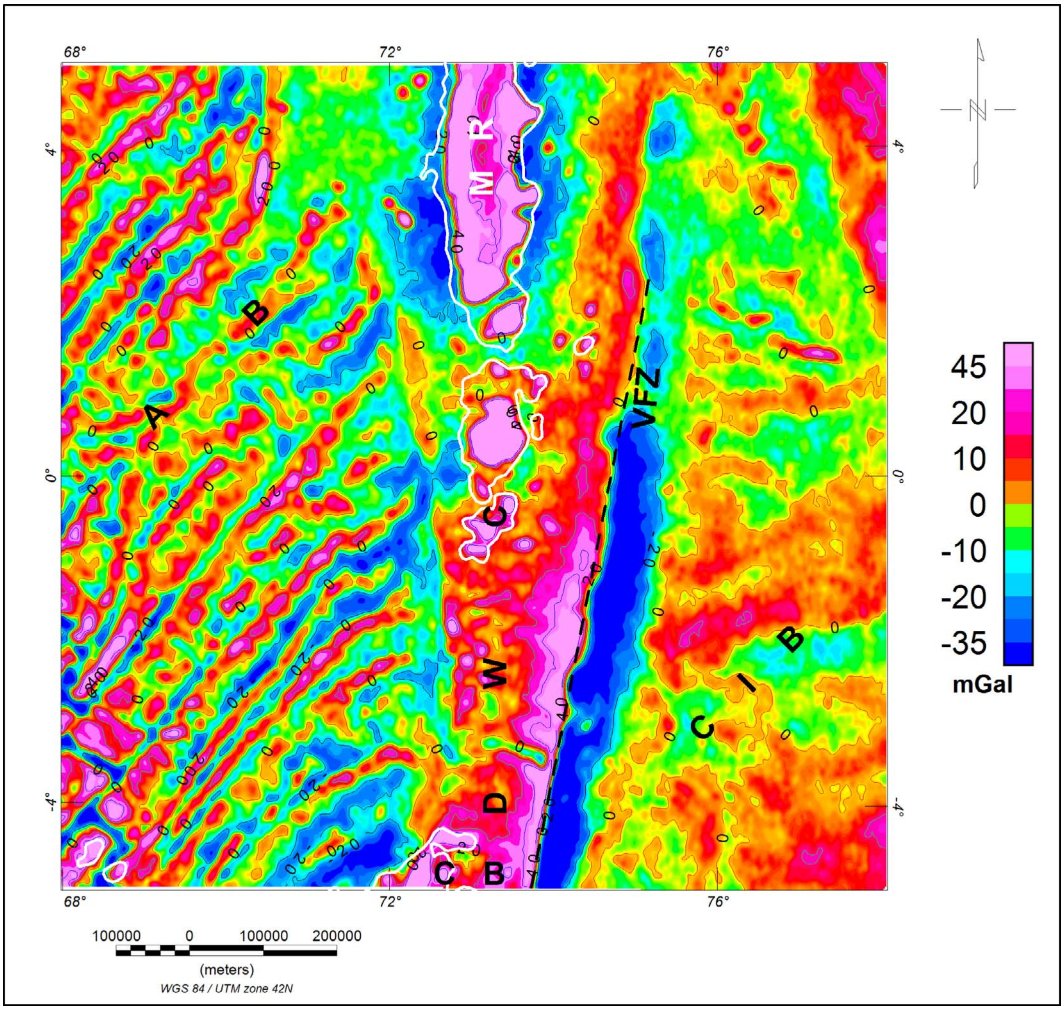

Fig. 2. Geoid corrected satellite derived free-air gravity anomaly map of the study region. The long wavelength gravity effect of Indian Ocean Geoidal Low (IOGL) is calculated using the spherical harmonic coefficient of EIGEN-6C4 (Förste et al., 2015) up to degree and order 50 and is removed from the FAG anomaly (V.24.1, Sandwell and Smith, 2009). **AB:** Arabian Basin, **MR:** Maldive Ridge, **DWC:** Deep Water Channel, **CB:** Chagos Bank (**GMR:** include MR, DWC, CB), **VFZ:** Vishnu Fracture Zone, **CIB:** Central Indian Basin, **GMR:** Greater Maldive Ridge. White lines show 2000 m isobath.

2014) to obtain FAG-IOGL map (Fig. 2).

The FAG-IOGL anomaly map includes the strong gravity effect of the water layer, consequently the FAG map shows strong correlation with bathymetry, which makes it difficult to judge if an observed anomaly is caused by a geological feature in the subsurface or by the seafloor topography. The FAG-IOGL maps mimic the bathymetry due to the large density contrast between seafloor and the overlying sediments. This dependency can be reduced by applying a Bouguer reduction to the FAG-IOGL data. The Bouguer anomaly can be correlated mainly with lateral density variations within the crust and Moho topography. To compute the Complete Bouguer Anomaly (CBA) from FAG-IOGL, the Fortran program FA2Boug (Fullea et al., 2008) which computes the complete Bouguer correction including the Bouguer plate, Curvature and Terrain correction, was utlized. The Bouguer plate correction is based on an infinite slab model by assuming the values of crustal and sea-water densities. A density of 1030 kg/m^3 and 2900 kg/m^3 was assumed, respectively for sea water and the crust. A density of 2900 kg/m^3 is assumed for the crustal part as the region under study is mostly occupied by oceanic crust as is evident from the seafloor spreading anomalies on either side of the Greater Maldive Ridge (Müller et al., 2008). The curvature correction takes into account the curvature of the earth's surface by modifying the infinite slab modelled with the plate correction to a spherical cap of approximate radius 167 km. The calculated values of curvature correction varies between -0.2 mGal to 5.5 mGal. The terrain correction minimizes the effect of extreme topographic reliefs, computed by considering each grid point in topography data as flat top of a squared prism (Fullea et al., 2008). The program computes terrain corrections for both the land and sea points in several spatial domains based on the distance between the topography and the calculation points. The limit and grid step used for the distant zone and intermediate zone are 167 km, 4 km and 20 km, 2 km respectively. The combined slab, curvature and terrain correction applied to the geoid corrected free air anomaly map (FAG-IOGL) provides the Complete Bouguer Anomaly (CBA) map (Fig. 3).

3.1. Moho depth estimation from gravity inversion

The Moho topography was initially computed by inverting the Complete Bouguer Anomaly without applying sediment and lithospheric thermal and pressure gravity corrections. This was followed by an estimation of Moho topography from Mantle Residual Gravity Anomalies (MRGA). Large-scale variations in MRGA reflect how the Moho undulates, because the Moho represents the largest density boundary in the lithosphere. To isolate the gravity anomaly caused only by the geometry of the Moho interface, all other contributions to the CBA anomaly must be removed. MRGA, which represents the gravity anomaly produced due to the geometry of the Moho interface, has been generated from the Complete Bouguer Gravity anomaly by removing

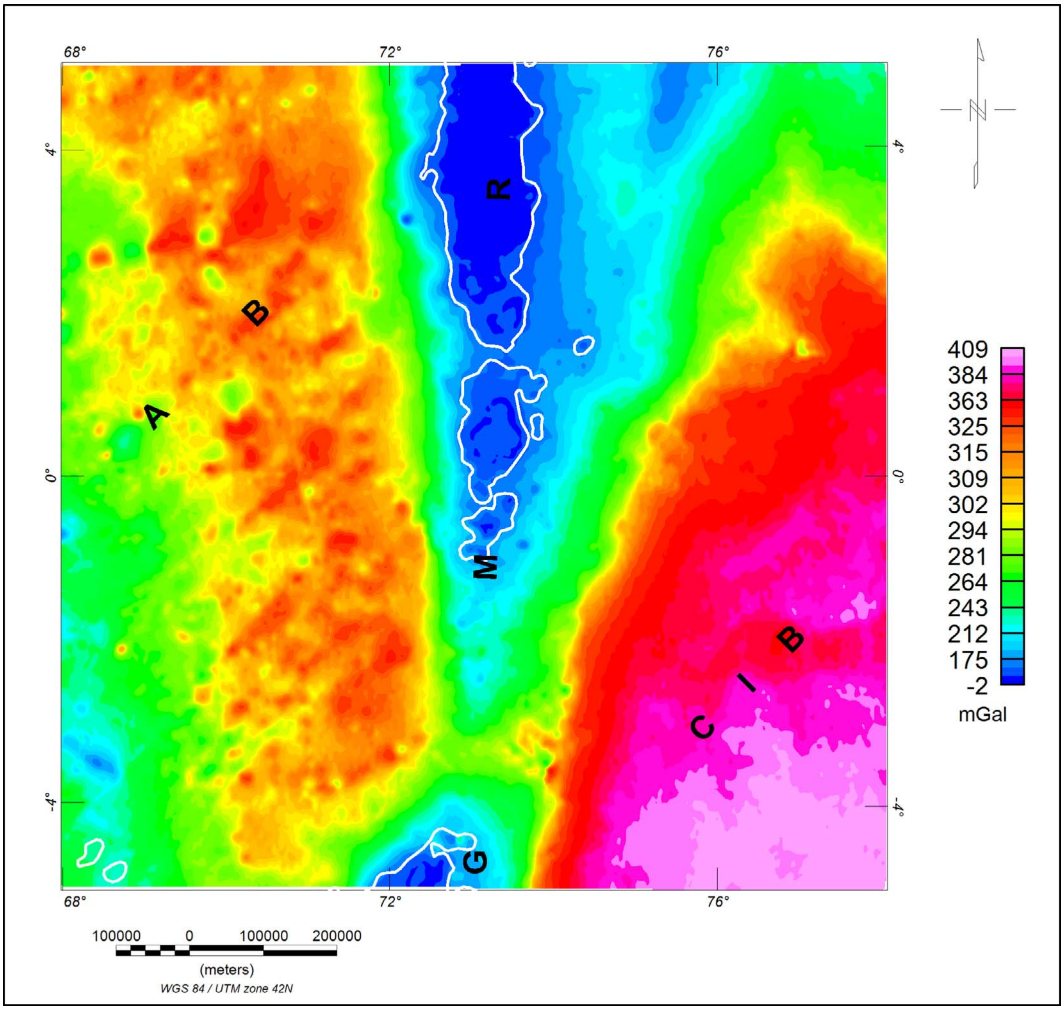

Fig. 3. The map showing the Complete Bouguer Gravity anomaly obtained after applying Bouguer plate, Curvature and Terrain correction to geoid corrected free air anomaly data. A density of 1030 kg/m^3 and 2900 kg/m^3 was assumed respectively for sea water and crust. **AB:** Arabian Basin, **CIB:** Central Indian Basin, **GMR:** Greater Maldive Ridge. White lines show 2000 m isobath.

the gravity effect of sediment layer and the gravity effects caused by temperature and pressure variations within the lithospheric mantle. The gravity effects of sediment layer and conduction dominated lithospheric mantle are computed by Fourier domain forward modelling methods (Parker, 1972; Blakely, 1995) which allows rapid computations of gravity fields caused by a non-uniform and uneven layer of material.

3.2. Sediment gravity correction

For estimating the gravity effect of sediments a variable density of sediment layer is considered based on the relationship between sediment thickness, porosity and density (Sawyer, 1985; Bai et al., 2014). The effect of sediment density is calculated using a relationship between sediment porosity (Φ_z) and the overlying sediment thickness (z) using the relation

$$\Phi_z = \Phi_o e^{-cz} \tag{1}$$

where Φ_o is the initial porosity and c is an empirically determined constant with unit 1/depth. If sedimentary pore space is filled by seawater, with z km overlying sediment, the density (ρ_z) will be (Sawyer, 1985).

$$\rho_z = \Phi_z \rho_w + (1-\Phi_z)\rho_{sg} \tag{2}$$

where ρ_w is the sea water density and ρ_{sg} is the grain density.

3.3. Gravity effect of lithospheric temperature and pressure variation

The lithosphere thermal gravity anomaly, caused by the lateral variation in lithospheric temperature is important in oceanic regions as it generates approximately −380 mGal (Greenhalgh and Kusznir, 2007) at the oceanic ridges and decays as one moves towards the rifted continental margin. Lithospheric thermal gravity correction is required to compensate for this large negative anomaly component arising from oceanic lithosphere having an elevated gradient that trend to predict Moho depths which are too large than the actual depths (Cowie and Kusznir, 2012). In the calculation of the lithospheric thermal gravity anomaly, the lithospheric temperature has to be initially calculated followed by the density perturbations due to oceanic lithosphere cooling effects which is then used to generate the lithospheric thermal gravity anomaly. The pure-shear model of McKenzie (1978) was used to generate the temperature field of the lithospheric mantle at depth z which is the vertical distance from the target point to the model basement, as given by the equation

$$Tz = T_l\left\{1-\frac{z}{a} + \frac{2}{\pi}\sum_{n=1}^{\infty}\frac{(-1)^{n+1}}{n}\left[\frac{\beta}{n\pi}\,sin\,\frac{n\pi}{\beta}\right] \times \exp\left(\frac{-n^2t}{\tau}\right)sin\frac{n\pi z}{a}\right\} \tag{3}$$

where T_l is the temperature at the base of the lithosphere, a is the depth to the base of the model, τ is the lithospheric cooling thermal decay constant, t is the crustal age and β is the lithospheric stretching factor whose value is infinity for oceanic area, unity for unstretched continental area and is equal to crustal stretching factor (i.e., the ratio of pre-stretching continental crustal thickness to present day crustal thickness) for stretched continental lithosphere.

The well identified marine magnetic lineation can be used to represent oceanic crustal age in estimating lithospheric thermal structure based on the plate cooling model (Bai et al., 2014). For this the oceanic crustal age grid of Müller et al. (2008) was utilized. The lithospheric density changes due to pressure compression driven by overburden stress can be modelled with the knowledge of compressibility coefficient (γ_T) which has a reciprocal relationship with bulk modulus K_T and pressure change at temperature T. The bulk moduli of forsterite, an abundant mineral in the upper mantle, can be linearly approximated as a function of temperature (Kroll et al., 2012)

$$K_T = 127.97 - 0.0232(T-300)$$

The lithospheric mantle density changes due to thermal expansion and pressure compression are then calculated using the relation

$$\rho_{TP} = \rho_0\,[1-\alpha(T)(T-T_0) + \gamma_T\,[P(z)-P_0]] \tag{4}$$

where $\alpha(T)$ is the thermal expansion coefficient, ρ_0 is the mantle density at normal temperature (T_0) and pressure (P_0), $P(z)$ is the pressure on the target point where the temperature is T.

3.4. Gravity inversion

In this study, the code developed by Gómez-Ortiz and Agarwal (2005) based on the wave number domain inversion scheme described by Oldenburg (1974) was used in order to determine the three dimensional geometry of the Moho interface from the gravity anomalies (CBA and MRGA), given by

$$F\,[h(x,y)] = -\frac{F\,[\Delta g(x,y)]\,e^{|k|z}}{2\pi G\rho} - \sum_{n=2}^{\infty}\frac{|k|^{n-1}}{n!}F\,[h^n(x,y)] \tag{5}$$

where $\boldsymbol{F}[\,]$ indicates the 2D discrete Fourier transform, $\boldsymbol{G}$ is the universal gravitational constant, ρ is the density of the interface, $\boldsymbol{\Delta g}(\boldsymbol{x},\boldsymbol{y})$ is the gridded gravity anomaly, $\boldsymbol{h}(\boldsymbol{x},\boldsymbol{y})$ is the depth to the interface, $\boldsymbol{z}$ is the mean depth of the horizontal interface and $|\boldsymbol{k}|$ is the absolute value of the wave vector. Given the mean depth of the density interface and density contrast associated with two media, the topography of the Moho surface is computed from the gravity anomaly by means of an iterative process (Chappell and Kusznir 2008; Bai et al., 2014). A cosine low pass filter was applied to the both CBA and MRGA before the inversion process to remove the short wavelength components within the data caused by shallow sources within the crust, so that the above equation will converge. Also, in order to fulfil Smith's (1961) uniqueness theorem the densities of the two overlying layers (for e.g. crust and mantle) have to be constant.

4. Free-air Anomaly, Complete Bouguer anomaly (CBA) and Moho topography

The FAG-IOGL (Fig. 2) anomaly map generated after removing the effect of IOGL (very long wavelength features) from FAG is represented as a histogram equalized colour shaded image (Geosoft, 2014) in which the warm and cool colours represent highs and lows, respectively. The moderate to long wavelength free air anomalies range in amplitude from approximately −75 mGal to 115 mGal. The Greater Maldive Ridge (GMR) region of the Chagos-Laccadive Ridge can be easily identified as N-S trending gravity feature compared with the surrounding oceanic regions. Over the GMR, the Maldive Ridge stands out as a long wavelength positive gravity feature along with few isolated positive anomaly closures. By and large, one can see a positive correlation between bathymetry and free air anomalies over the ridge. The complexity of the free air anomalies appears to differ on either side of the GMR. Towards the west of the GMR (Fig. 2), in the Arabian Basin, NE-SW tending linear anomalies representing the fracture zones are clearly evident. In the Central Indian Basin, towards the east, the anomalies are subdued without any regular trend/pattern. A N-S trending low observed on the eastern flank of the GMR can be associated with the Vishnu Fracture Zone (VFZ) (Whitmarsh, 1974) which was interpreted to form an abrupt boundary between younger ocean floor in the west and older towards the east implying scope for sedimentary pile on the older ocean floor for petroleum exploration (Nathaniel, 2011; Kalra et al., 2014).

The Complete Bouguer Anomaly map (Fig. 3) generated from FAG-IOGL map is dominated by medium to long wavelength anomalies with amplitude ranging from approximately −2 mGal to ~400 mGal. The anomaly shows relatively low amplitudes over the GMR compared to the adjacent ocean floor which shows high amplitudes. Large positive anomalies are associated with regions where the crust is very thin (Lowrie, 2007). The gravity anomaly signatures representing the oceanic fracture zones observed in the FAG-IOGL is not very evident in the CBA map. Bouguer anomaly amplitudes in the Central Indian Basin are higher compared to the Arabian Basin. The southern part of the Central Indian Basin shows anomalies of the order of 350–400 mGal while the anomalies in the Arabian Basin ranges from 25 to 300 mGal.

The CBA was initially inverted to generate the Moho undulations without applying the sediment and lithospheric thermal and pressure corrections. Two input parameters required for the inversion of gravity anomalies to obtain Moho undulations are density contrast and mean Moho depth. A mean Moho depth of 12 km, from CRUST 1.0 (Laske et al., 2013) and the Moho depths from seismic refraction stations (Francis and Shor, 1966) of the adjoining areas (for location refer Fig. 1) and a density contrast of 400 kg/m^3, is assumed for the first iteration. A density of 3300 kg/m^3 was assigned for mantle, and 2900 kg/m^3 for crust as the region under study is mostly covered by oceanic crust. The inversion converged after 9 iterations. The Moho undulations thus inverted from CBA is shown in Fig. 4 which gives an average Moho depth of approximately 17 km underneath the GMR reaching to a maximum of over 26 km below the Maldive Ridge crest. It can be observed that the Moho is shallowing on either side of the ridge in the ocean basins. The computed Moho depth in the Arabian Basin with a mean value of 11 km is relatively thicker than the Central Indian Basin (mean thickness 8 km).

To compute the gravity anomalies generated by the sedimentary column, the total sediment thickness grid of the world oceans, version 2 (Whittaker et al., 2013; Divins, 2003) from NOAA/NGDC was utilized. The sediments thickness model has an average vertical resolution of 50 m and a horizontal dimension of 5.5 km × 5.5 km. The sediment density for each grid of the model is calculated using Eqs. (1) and (2). The porosity values were taken from the ODP Leg115 (Backman et al., 1988) sites 710 and 711 (location shown in Fig. 1). Porosity values from sites 712 to 716 were not considered as these are over the Maldive Ridge and may not represent average values. Even though sites 710 and 711, are located in the Eastern Somali Basin, the porosity values of these locations were selected as these occur at an average water depth of 4 km and the average water depth of major part of the region under study is also, approximately 4 km. In addition, these cores are from an ocean floor of approximately 50 Ma which also matches with the average age of the ocean floor in the study region. An exponential fit to the plot of porosity vs depth is shown in Fig. 5 from which the constant c is found to be 6.47×10^{-4}/m and the initial porosity Φ_o is 0.7468. Utilizing the initial porosity value and c, thus obtained from the best exponential fit, porosity values at different depths (Φ_z) is computed using Eq. (1) and the densities of different layers of the sedimentary column was computed using Eq. (2). Density of pore fluid is assumed to be 1030 kg/m^3 and grain density 2694 kg/m^3, average values of grain density from ODP wells 710 and 711 (Backman et al., 1988). Using

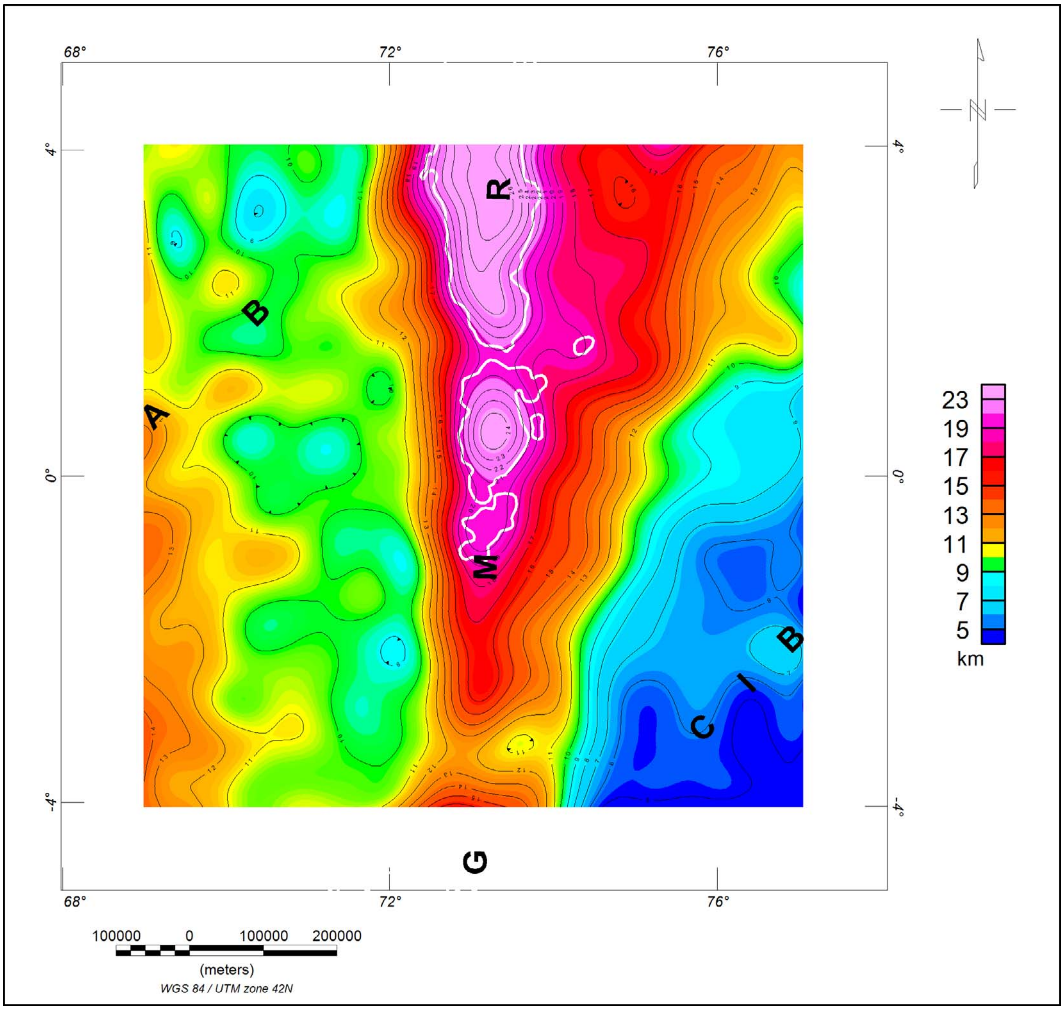

Fig. 4. Moho depth variation derived from Complete Bouguer Gravity anomaly without sediment and lithospheric mantle temperature-pressure correction. **AB:** Arabian Basin, **CIB:** Central Indian Basin, **GMR:** Greater Maldive Ridge. White lines show 2000 m isobath.

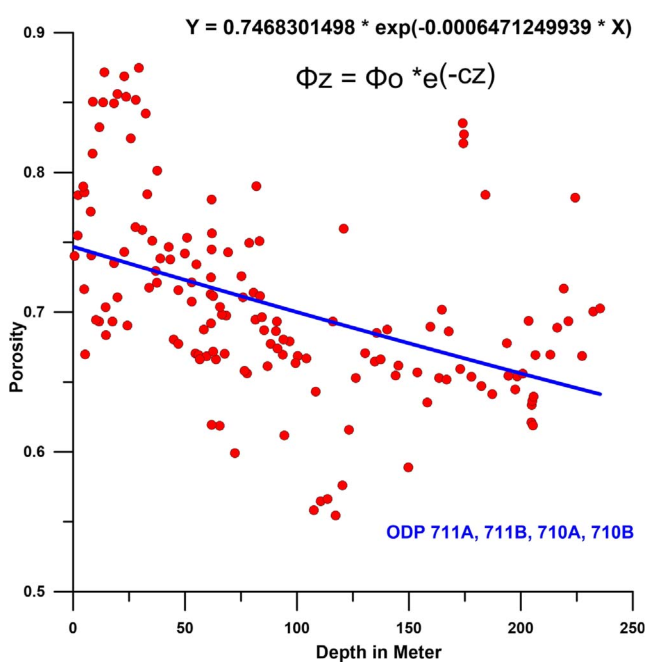

Fig. 5. Porosity vs depth plot of ODP wells 710 & 711 (Backman et al., 1988). The dark blue line represents the exponential fit to the plot. (For interpretation of the references to colour in this figure legend, the reader is referred to the web version of this article.)

these computed density values the total gravity effect arising from the sediments is calculated whose mean value is found to be ∼10 mGal.

The density of the lithosphere arising from thermal expansion and pressure changes, was computed using Eq. (4) for a three dimensional grid with horizontal dimensions of 5.5 km × 5.5 km and average vertical spacing of 6 km. The thermal expansion coefficient $\alpha(T)$ was assumed to be $3.28 \times 10^{-5}\mathrm{K}^{-1}$ (Greenhalgh and Kusznir, 2007) and the mantle density ρ_0 at normal temperature (T_0 = 273K) and normal pressure (P_0, standard atmospheric pressure) to be 3300 kg/m^3. The lithospheric stretching factor, β (set at infinity as the region under study is mostly oceanic) and the lithospheric thermal equilibration time, t, are the two unknown factor in Eq. (3). Lithospheric thermal equilibration time, t, is obtained from the oceanic crustal age grid of Müller et al. (2008). Values of 62.8 and 125 km (Ma and Dalton, 2017) was taken respectively for thermal decay constant (τ) and depth to base of lithosphere (a). The temperature at the base of the lithosphere (T_1) is taken to be 1450 °C as given by Ma and Dalton (2017) through analysis of Rayleigh wave phase velocity maps for the northern Indian Ocean. The combined effect of sediment and lithospheric thermal and pressure gravity anomalies thus calculated is removed from the Complete Bouguer Anomaly to obtain the Mantle Residual Gravity Anomalies (MRGA) represented in Fig. 6. The MRGA anomalies are then inverted using Eq. (5) assuming a density contrast of 400 kg/m^3 and an initial mean Moho depth of 12 km (average assumed from CRUST1.0 model and available seismic refraction data from the adjoining regions). A Cosine taper low pass filter with frequency roll-off from 75 to 150 km

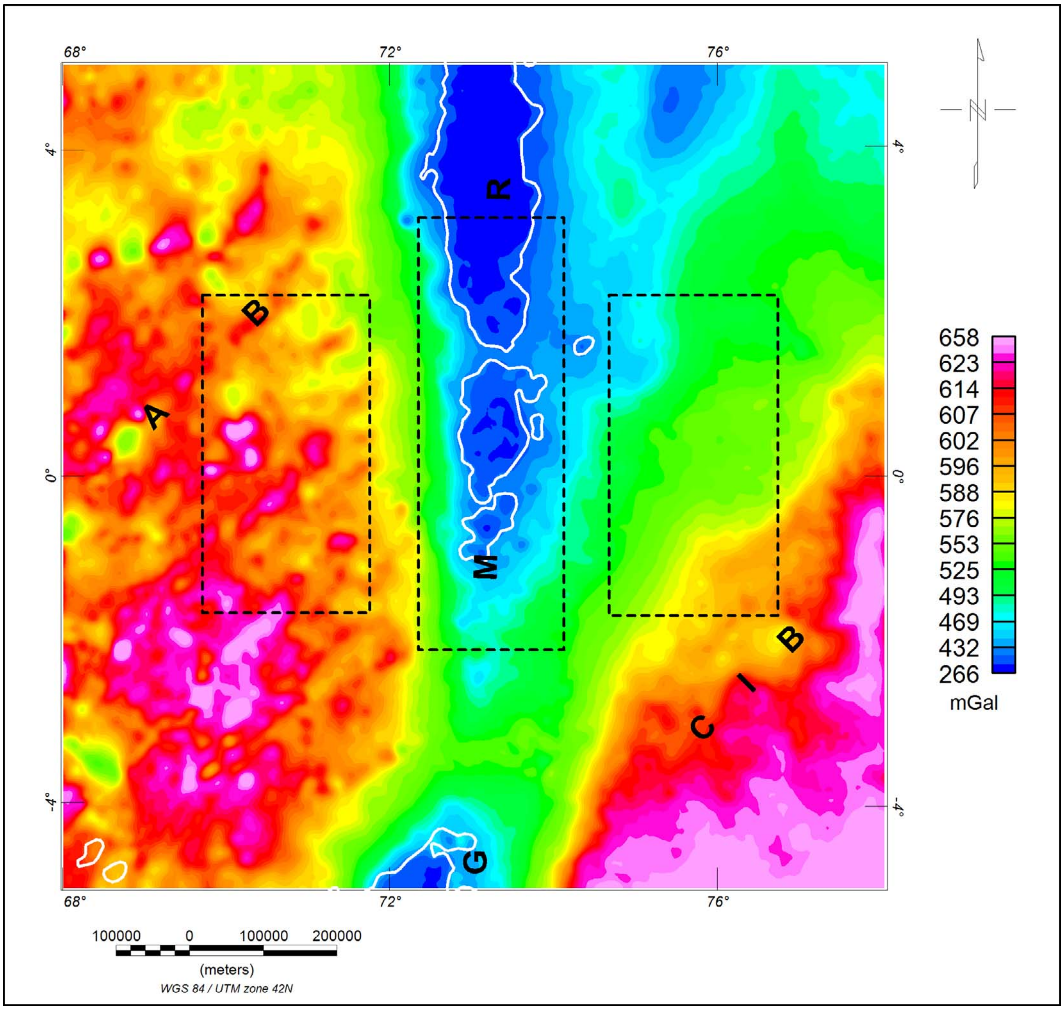

Fig. 6. Mantle Residual Gravity Anomaly obtained after removing the gravity effect due to bathymetry, sediment and lithospheric mantle temperature-pressure variation. The dashed rectangles mark out the three regions, Western block (Arabian Basin), Middle Block (Maldive Ridge) and Eastern Block (Central Indian Basin) used in Fig. 9. **AB:** Arabian Basin, **CIB:** Central Indian Basin, **GMR:** Greater Maldive Ridge. White lines show 2000 m isobath.

was applied to both CBA and MRGA anomalies before inversion to remove the effect of shallow sources originating within the crust so that equation can converge. The Moho undulation obtained after the convergence of iterations is shown in Fig. 7. There is striking difference in the Moho undulations computed from CBA and MRGA. From the Moho topography generated from MRGA (we call this as Final Moho), it can be seen that the Arabian Basin is comparatively thinner than the Central Indian Basin which was reverse in the case of Moho undulations computed from CBA. This shows the necessity of incorporating the gravity effect from sediments as well as the lithospheric thermal and pressure anomalies in computing the Moho variation. There is no significant variation of Moho topography over the GMR computed using the different data set. Crustal thickness map (Fig. 8) was generated by removing the total thickness of bathymetry and sediments from the Moho topography.

In the pure shear model (McKenzie, 1978, McKenzie et al., 2005) used in the present study for deriving the thermal and pressure induced gravity anomalies, there are different sets of parameters used to obtain the temperature field of lithospheric mantle (refer Eq. (3)). Since there is no measured quantities of these parameters in the region under study, the model parameters have been tested by varying the parameters over a range of values from similar studies in other regions. The values obtained by Parsons and Sclater (1977) for the North Pacific were a = 125, T_1 = 1333 °C, $\alpha(T) = 3.28 \times 10^{-5}\,K^{-1}$ while that deduced for the same region by Stein and Stein (1992) are a = 95 km, T_1 = 1450 °C and $\alpha(T) = 3.138 \times 10^{-5}K^{-1}$. For thermal corrections, in the NE Atlantic region, the values used were a = 125 km, $\alpha(T) = 3.28 \times 10^{-5}\,K^{-1}$, T_1 = 1300 and τ = 62.8 Ma by Greenhalgh and Kusznir (2007) while for eastern and southeastern Asia, Li and Wang (2016) assumed values of a = 95 km, T_1 = 1300 °C and $\alpha(T) = 2.55 \times 10^{-5}K^{-1}$. Bai et al. (2014) assumed values of a = 125 km, T_1 = 1333 °C, τ = 62.8 Ma and $\alpha(T) = 3.28 \times 10^{-5}\,K^{-1}$ for obtaining the thermal gravity anomalies in the south China sea. For the present study thickness of the lithosphere (a) and temperature at the base of lithosphere (T_1) is taken as 125 km and 1450° C respectively as reported by Ma and Dalton (2017) for northern Indian Ocean through analysis of Rayleigh wave phase velocity maps while τ and $\alpha(T)$ where assumed to be 62.8 Ma and $3.28 \times 10^{-5}\,K^{-1}$. Since exact values of these parameters are not known, range of values of these parameters were considered and the Moho depths were calculated varying each parameter at a time. The result of this exercise is shown in Fig. 9. The region was divided into three blocks (superposed in Fig. 6), Western Block (Arabian Basin), Middle Block (Maldive Ridge) and Eastern Block (Central Indian Basin) to see how the average Moho depth in each block is affected as the parameters are varied. The parameter value used for the present calculation is represented by a star in each of the blocks. Lithospheric base depth (a), $\alpha(T)$ and τ were varied for two lithospheric base temperatures 1333 °C (dotted line) and 1450° (continuous line) as shown in Fig. 9. The maximum and minimum values obtained for each block is shown in the Table 1. For any given parameter, the variation in Moho

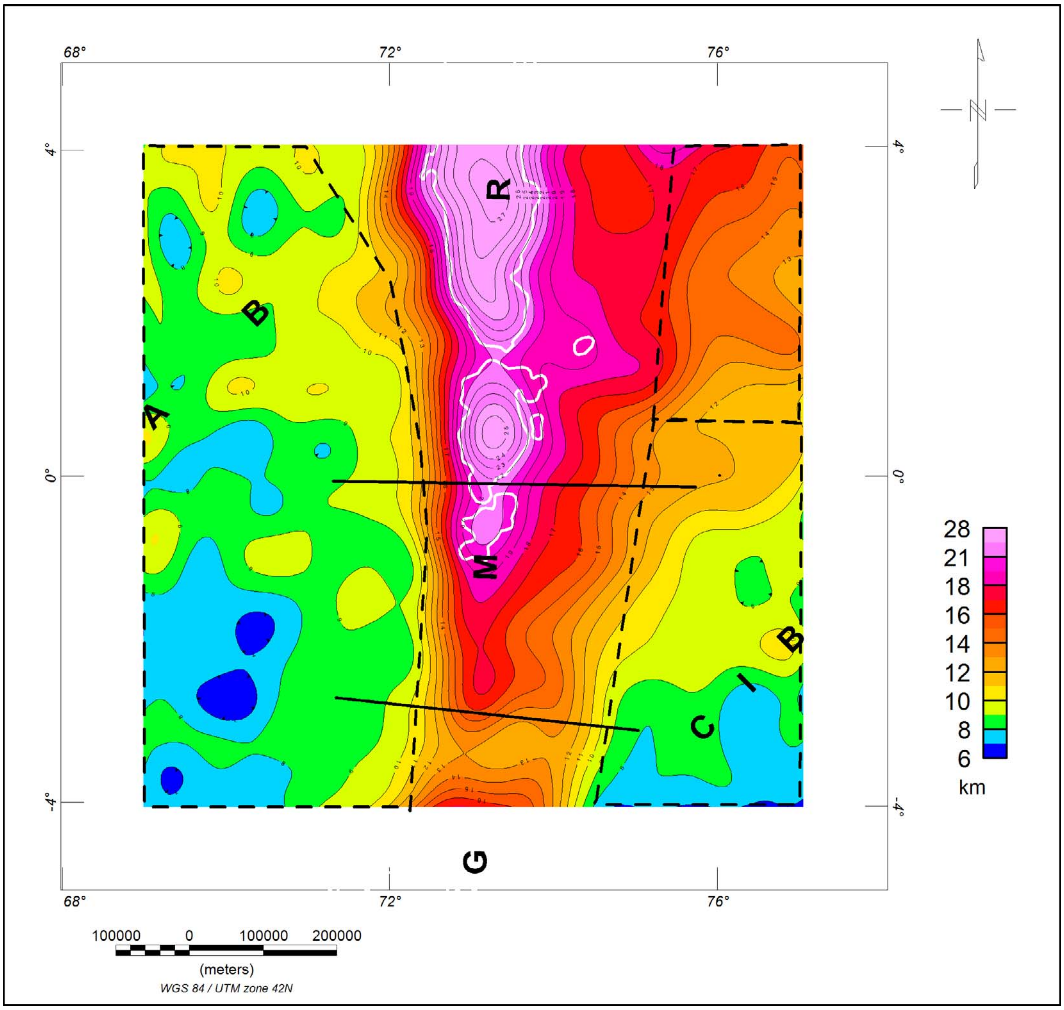

Fig. 7. Predicted Moho depth from the inversion of Mantle Residual Gravity Anomaly. The dashed polygons show the regions used for calculating the average Moho depths in the Arabian Basin (**AB**) and Central Indian Basin (**CIB**). **GMR:** Greater Maldive Ridge. White lines show 2000 m isobath. Black lines: Gravity profiles analyzed by Henstock and Thompson (2004).

depth arising from the base temperature (T_1) variation is marginal. As can be seen from the figure, Moho depths of the Western and Eastern blocks show opposite trend for any given parameter. Change in depth to the base of the lithosphere (a) and τ (lithospheric cooling thermal decay constant) have very little effect on depth to Moho while a large variation of more than a kilometer is seen in Moho depths as the thermal expansion coefficient ($\alpha(T)$) is varied. These tests suggests that the Moho variations are not significantly controlled by the studied parameters used to compute the lithospheric thermal gravity anomalies.

In addition to varying the parameters used for calculating the lithospheric thermal and pressure related gravity anomalies, Moho depths were also calculated (a) without considering the effect of sediments but retaining the lithospheric temperature and pressure related terms and (b) without the pressure term but keeping the sediment thickness and lithospheric temperature terms. These are shown in Fig. 10.

5. Discussion

In the present work, the Moho undulations below the Greater Maldive Ridge (GMR) segment of the Chagos-Laccadive Ridge and adjoining oceanic areas were estimated through gravity inversion technique incorporating lithospheric thermal and pressure anomaly correction in addition to bathymetry and sediment corrections. The estimated Moho depths range from 7 km to 28 km and the crustal thickness from 2 km to 27 km. The Moho depths are shallower in regions closer to young spreading center (Central Indian Ridge) in the Arabian Basin i.e., the region to the west of the GMR is thinner compared to the east. The thickest crust and the deepest Moho is found below the N-S trending Greater Maldive Ridge of the Chagos-Laccadive Ridge. Three E-W profiles cutting across the GMR and one N-S profile along GMR were extracted to compare the crustal thickness and Moho variations from west to east and north to south respectively (location of profiles superposed on Fig. 8). Each profile in Fig. 10 shows bathymetry, sediment thickness and Moho undulations calculated (i) directly from the inversion of Complete Bouguer Anomalies (CBA), (ii) after applying sediment and lithospheric thermal-pressure corrections (Final Moho), (iii) without sediment correction but with lithospheric thermal-pressure corrections, and (iv) with sediment and temperature correction but no pressure corrections. Before applying the sediment and temperature-pressure corrections, Moho was deeper in the younger Arabian Basin compared to the relatively older Central Indian Basin. This suggests the importance of lithospheric thermal-pressure anomaly corrections in estimating Moho depths or crustal thickness. But there is not much variation in the Moho undulations or crustal thickness over the GMR estimated with and without the sediment and thermal corrections which suggest that the crustal thickness of the ridge does not depend on the Ocean age isochrones (Torsvik et al., 2013) used to estimate the lithospheric thermal anomaly. The marginal difference seen can be attributed to the incorrect porosity, density and sediment thickness used to estimate the sediment gravity effect as the porosity values used for estimating the density is from the Eastern Somali Basin

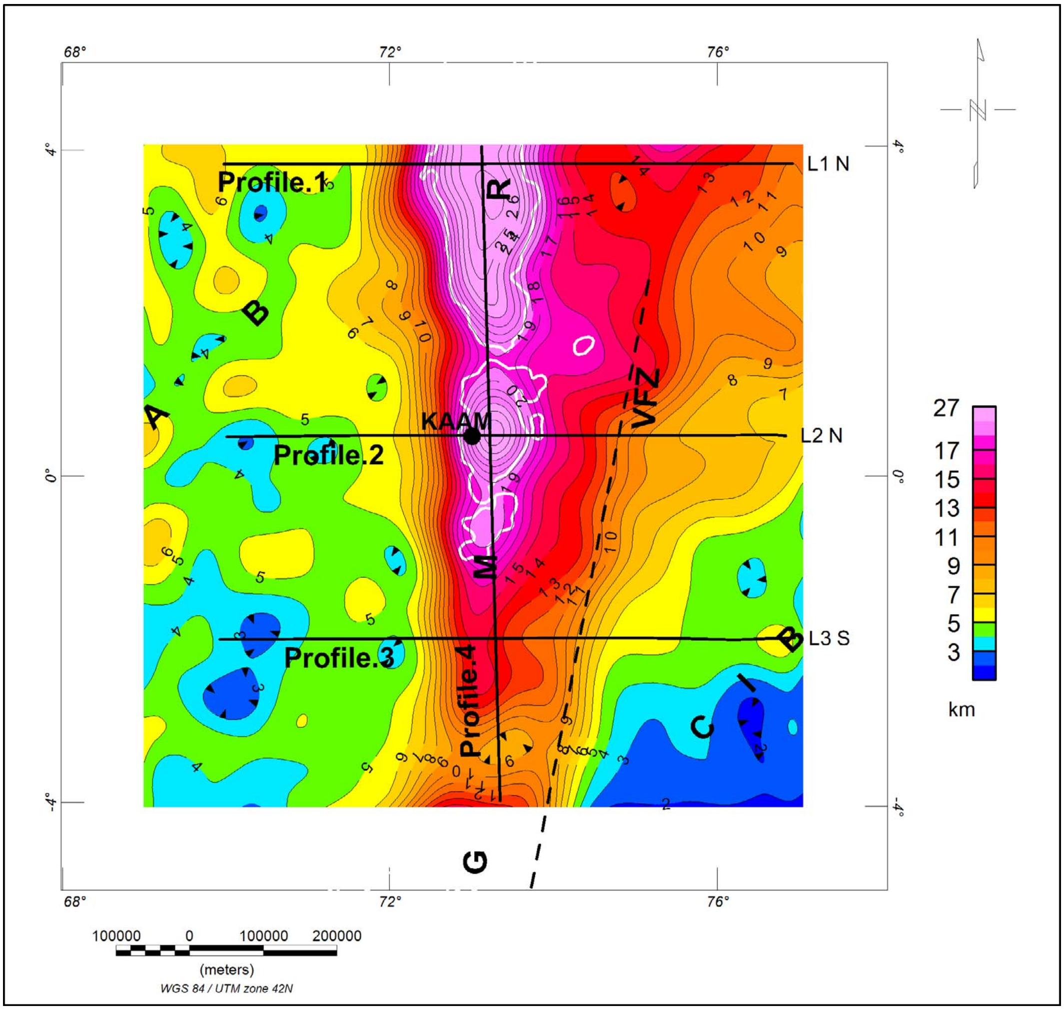

Fig. 8. The Crustal thickness map generated from the present study showing the locations of four profiles used for comparison of results shown in Fig. 10. The black solid circle labelled as KAAM marks the location of permanent broadband seismic station where the Moho depth is available from receiver function studies (Fontaine et al., 2015). **AB:** Arabian Basin, **CIB:** Central Indian Basin, **GMR:** Greater Maldive Ridge, **VFZ:** Vishnu Fracture Zone. White lines show 2000 m isobath.

(ODP Leg 710-711).

Receiver Function (RF) studies from permanent broadband seismic station KAAM on Maldive Ridge (Fontaine et al., 2015), location shown in Fig. 8, determined Moho depth below the station as 23 km. This station falls in the study area and hence a comparison of the results obtained from gravity inversion with that deduced from RF analysis could be undertaken. The Moho depth obtained from inversion of CBA for this location is 22.5 km while that obtained from Final Moho is 23.3 km. Both the values are very close to that obtained from the RF analysis. Mean Moho depth estimated from RF analysis over broadband station HMDM and LAK (Fontaine et al., 2015, Gupta et al., 2010) located over the northern part of the Maldive Ridge (refer Fig. 1 for location) are respectively 28 km and 24 km. The mean depth to Moho obtained for Arabian Basin from the present study (8.8 km) matched very well with the mean depth (8.9 km) from seismic refraction studies (Francis and Shor, 1966) (average of Moho depths from refraction stations 2,3,10 location in Fig. 1). Three seismic refraction stations (Francis and Shor, 1966) were acquired along the axis of the CLR whose locations are shown in the Fig. 1. Of these, Station-1 is located north of the present study region (midway between Maldive Ridge and Laccadive Plateau) while 4 and 5 falls in the channel between Maldive Ridge and Chagos Bank. The crustal thickness revealed along Station-1 is 10 km and Moho depth is 17 km. Beneath the refraction stations 4&5, no mantle arrivals were observed based on which a Moho depth of at least 20 km was suggested by Francis and Shor (1966). In this region, from self-consistent modelling of gravity and bathymetric data (profile location shown in Fig. 7), Henstock and Thompson (2004) computed mean crustal thickness of 12.5 km. Crustal thickness estimated from the present study at these station locations is approximately 13 km. The average depth to Moho in the Central Indian Basin (CIB) (from refraction stations 6,7 located marginally south of the study area) is about 10 km while that obtained from the present analysis is about 12 km. Refraction studies in the Arabian Basin (AB) (stations 2,3,10) gave an average Moho depth of 9 km while that computed from the inversion of Mantle Residual Gravity Anomalies is ~8.8 km. The average Moho depth for the Arabian Basin and CIB were respectively about 10.6 km and 9.5 km before the sediment and lithospheric temperature-pressure corrections were applied. The area used to calculate the average depths in the AB and CIB Basin is shown in Fig. 7. Thus, the Moho depth and crustal thickness estimated from the inversion of gravity data, after applying lithospheric thermal-pressure gravity anomalies and sediment correction, matches reasonably well with the depths obtained from the limited previous geophysical surveys over Maldive Ridge and adjoining ocean basins.

Some interesting facts emerge from analysis of profiles 1 to 4 (shown in Fig. 10). In both, crustal thickness as well as Moho undulation maps, there is a sharp boundary between the Arabian Basin and the GMR suggesting a deep seated fault while the contact between GMR and Central Indian Basin (CIB) is more gradational. The average difference in Moho discontinuities observed beneath the Greater Maldive

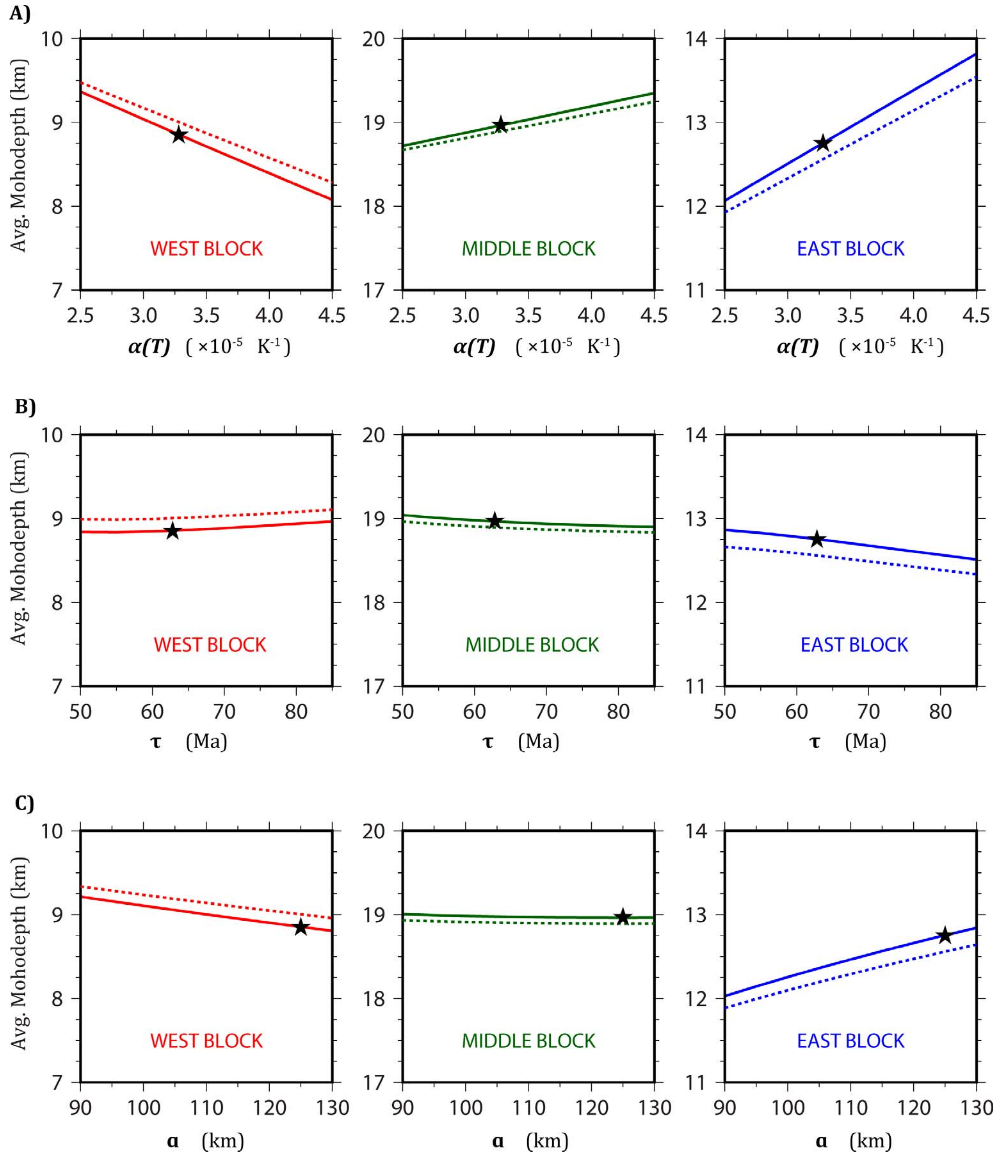

Fig. 9. Variation of Average Moho depth over Western block, Middle Block and Eastern Block for a range of values of **A)** Thermal expansion coefficient $\alpha(T)$, **B)** Lithospheric cooling thermal decay constant (τ) and **C)** Depth to the base of the model (a) for two lithospheric base temperatures 1333 °C (dotted line) and 1450° (continuous line). The star represents the corresponding parameter value used in the present study. The boundary of the western, middle and eastern blocks are shown in Fig. 6.

Table 1
Variation of Moho depth estimated by changing the values of different parameters used in lithospheric thermal and pressure gravity correction. T_1 represents the temperature at the base of the lithosphere. GMR is Greater Maldive Ridge. The location of the blocks are shown in Fig. 6.

T_1	Western Block (Arabian Basin)		Middle Block (GMR)		Eastern Block (Central Indian Basin)	
	Minimum	Maximum	Minimum	Maximum	Minimum	Maximum
Varying thermal expansion coefficient α(T)						
1450	8.1	9.4	18.7	19.4	12.1	13.8
1333	8.3	9.5	18.7	19.3	11.9	13.5
Varying Lithospheric cooling thermal decay constant (τ)						
1450	8.8	9.0	18.9	19.0	12.5	12.9
1333	9.0	9.1	18.8	19.0	12.3	12.7
Varying Depth to the base of the model (a)						
1450	8.8	9.2	19.0	19.0	12.0	12.8
1333	9.0	9.3	19.0	18.9	11.9	12.6

Ridge (GMR) and AB is about 10 km while that between GMR and CIB is approximately 7 km. The average crustal thickness is more in the CIB compared to AB after the sediment and lithospheric thermal and pressure corrections has been incorporated which is in accordance with the age of the basin. But within the Central Indian Basin, crustal thickness decreases from north to south with the average thickness being ~13 km along Prof.1 reducing to 5 km along Prof.3 through 7.6 km in Prof.2. In the Arabian Basin the crustal thickness reduces from average 5.5 km along Prof.1 to 3.8 km along Prof.3 which is very close to the spreading Central Indian Ridge. The magnetic isochrons in the Arabian Basin suggests ages between 5 and 45 Ma while that in the Central India Basin ranges from 70 to 80 as per the age grid of Müller et al. (2008). The CIB, the region to the east of the Vishnu Fracture Zone (VFZ), was divided into northern and southern segments, the divide being slightly north of 0°N where the NE-SW trending FAG-IOGL anomaly low associated with VFZ shows a break. The average crustal thickness and Moho depth of the northern segment are respectively 10.3 and 14.3 km while that of the southern segment is 4.7 and 9.6 km. The crustal thickness obtained from direct inversion of CBA for the northern segment is 7.9 km and southern segment is ~2 km which may be unrealistic for an oceanic

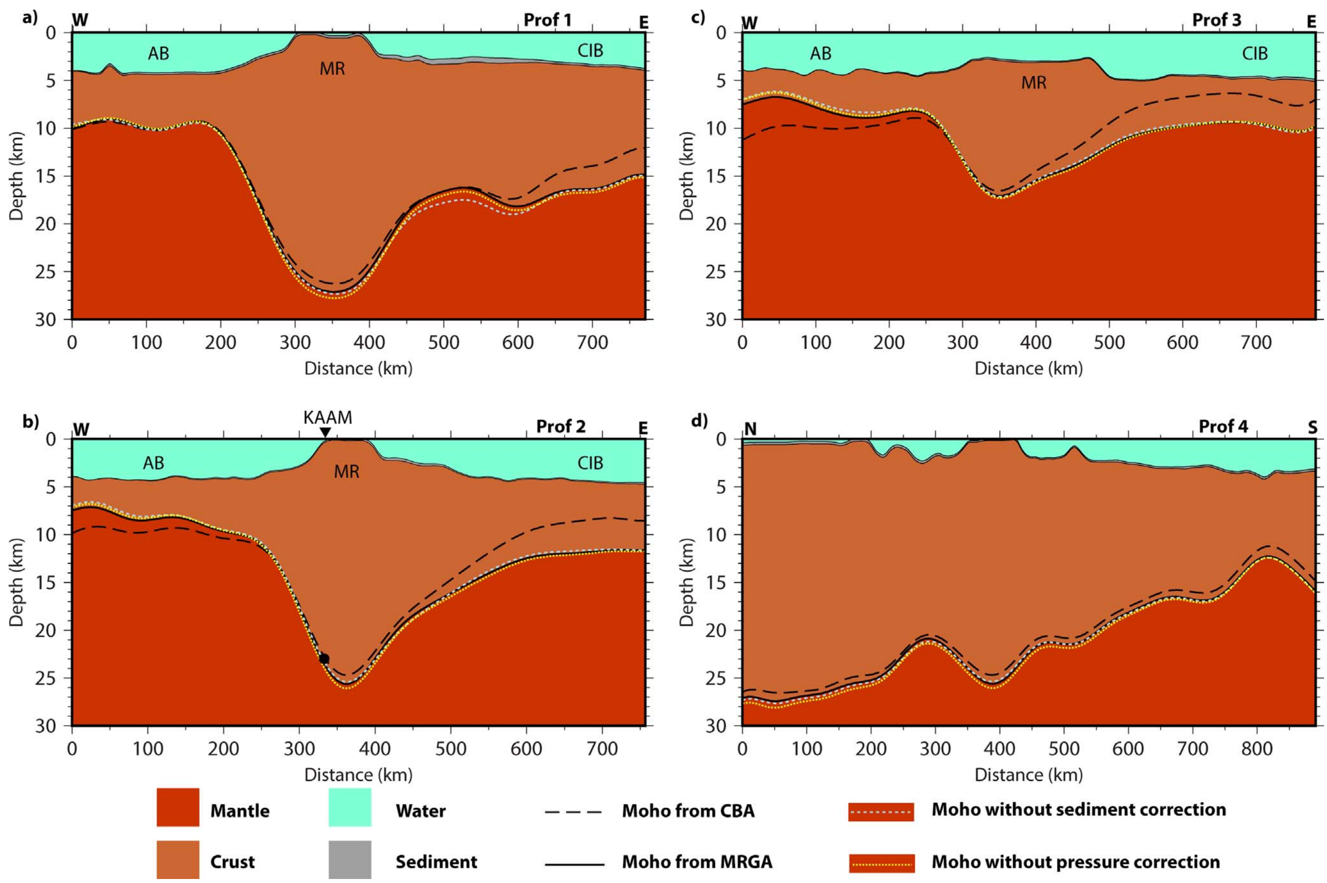

Fig. 10. Crustal thickness and Moho undulations along selected profiles computed: (i) from Mantle Residual Gravity Anomaly (black solid line), (ii) from Complete Bouguer Anomalies (black dashed line), (iii) without sediment correction but retaining the lithospheric temperature and pressure correction (blue small-dashed line), (iv) without the lithospheric pressure correction keeping the sediment and lithospheric temperature correction (yellow dotted line) – along three East-West profiles (a, b & c) and North-South profile (d). The locations of the profiles and the permanent seismic station KAAM marked as solid triangle in (b) are superposed in Fig. 8. The black solid circle in prof.2 represents the Moho depth derived through receiver function studies (Fontaine et al., 2015). (For interpretation of the references to colour in this figure legend, the reader is referred to the web version of this article.)

crust of ~80 Ma. The age dependent temperature-pressure anomaly corrections improved the crustal thickness estimate in the southern segment. The oldest magnetic isochron identified in the Central Indian Basin is A34 (approximately around 0°N latitude) corresponding to 83.64 Ma (Cande and Patriat, 2015). No clear isochrons were identified in the region above 0°N latitude (within the CIB), above which the crustal thickness also increases. If the region to the north of 0°N latitude is underlain by oceanic crust, it might have formed during the Cretaceous long normal Superchron which may be the reason why no sea floor spreading anomalies are identified. Assuming that the crust, north of 0°N, is formed during the Cretaceous Superchron the estimated average thickness of 10.3 km is comparatively higher for an oceanic crust (White et al., 1992) while the crustal thickness of 7.9 km (obtained before sediment, lithospheric-pressure-temperature correction) appears more meaningful. It can be seen from Fig. 10 that sediment and pressure corrections have marginal effect on the crustal thickness in the northern segment. Even with changing (lowering) the thermal expansion coefficient, the estimated crustal thickness will reduce by less than 1 km. This means that the increased crustal thickness in the northern segment of CIB has to be associated with the overall tectonic activity that has shaped this part of the Indian Ocean lithosphere. Two possibilities can be considered for the increased crustal thickness in the northern segment of CIB (a) as the sediment-thermal anomaly corrections increased the crustal thickness, for this segment of the CIB the age dependent correction may not be required which implies that this region may not be underlain by oceanic crust but a reworked/stretched continental crust and (b) if the thickness estimated after applying the correction is correct, then it is possible that the region may be underlained by oceanic crust, probably thickened due to underplating. In this region, there is other data available to verify these two possibilities. Seismic refraction stations (6, 7) (Francis and Shor, 1966) in the southern segment of CIB has shown a layer of thickness 1.3 km with velocity 5 km/s overlying a layer with ~4 km thickness and velocity of 6.69 km/s followed by a 7.78 km/s layer at a depth of 10 km. These layers may respectively represent Oceanic Layer 2, Layer 3 and Moho. The refraction stations does not provide any evidence of underplating (velocities of the order of 7.1–7.5 km/s is assumed to represent underplated material (for eg. Leahy et al., 2010)) in the southern segment where well defined sea floor spreading anomalies were identified. This mean that if underplating is the reason for the increased crustal thickness in the northern segment of CIB, the underplated material might have emplaced prior to the formation of the oceanic crust in the southern segment ie., before 83 Ma. Indian plate has witnessed two major hotspot activity (Müller et al., 1993) viz., the Marion and Reunion that led to the separation of India from Madagascar and Seychelles. These two hotspot activity have pivotal role in shaping the present crust in the study region. Paleomagnetic, geochemical and dating of rock samples from India and Madagascar (Radhakrishna and Joseph, 2012), which were considered as products of the Marion hotspot and associated volcanism responsible for the separation of Madagascar from India, suggested the breakup age to be around 90 Ma (Torsvik et al., 2000). Hence if underplating can be considered as the cause of the increased crustal thickness in the northern segment of CIB, then the underplated material might have been derived from the Marion hotspot activity. Previous studies have reported magmatic underplating associated with Reunion plume throughout the length of the

CLR (Fontaine et al., 2015, Gupta et al., 2010). This also throws light on the possibility of Vishnu Fracture Zone in controlling the magmatic underplating of the region ie., towards the west of VFZ underplating is derived from Reunion activity while in the east its derived from the Marion plume. Even though the above discussion mainly concentrated assuming an oceanic crust in the northern segment of CIB, the possibility of a stretched, reworked continental crust (Naini and Talwani, 1983) in this segment cannot be ruled out. 2D modeling of gravity and magnetic data along a profile with constrains from seismic data, cutting across the VFZ, around 7°N latitude, suggests transitional intruded crust in the region (Kalra et al., 2014). Further studies are required to prove either of the possibilities from the present study, discussed above. It is worth mentioning that the possibility of a basaltic flow over an existing crust has not been considered in the discussions.

Receiver function analysis has shown that the Moho depth decreases from north to south over the Chagos Laccadive Ridge being 24 km (Gupta et al., 2010) and 28 km beneath LAK and HMDM station to 23 km over KAAM station over Maldive Ridge to as low as 17 km over DGAR station in the Chagos Bank (Fontaine et al., 2015). The Moho depth over the Greater Maldive Ridge computed from the present study decreases from ∼27 km towards north to ∼17 km towards the south (Fig. 10d). From the analysis of receiver functions Fontaine et al. (2015) has shown that the initial Moho depth (before the formation of underplated rocks) below the Maldive island (station KAAM) was at 13 km as at this depth the shear wave velocity is between 4.4 and 4.6 km^{-1}. Similarly, beneath station HMDM the initial Moho was inferred to lie at a depth of 14 km. Similar studies at station LAK over the Minicoy islands (Gupta et al., 2010) have suggested initial Moho depths to lie at 16 km. In all these stations, the additional thickness was attributed to the magmatic underplated rocks as evidenced from the change in velocity of the shear waves. The forgoing discussions suggests that the present Moho discontinuity along the Chagos-Maldive-Laccadive Ridge axis lies at an approximate depth of 20 km beneath the surface, and appears, therefore, to be intermediate between the average Moho depths characterizing oceans and continents. Effective elastic thickness of the lithosphere computed through transfer function analysis of bathymetric and free air gravity data (Ashalatha et al., 1991, Tiwari et al., 2007) propose that the CLR is compensated locally and that the volcanism was emplaced on lithosphere with low Te values of 4 ± 2 km, suggesting its proximity to the mid-oceanic ridge during its formation. However, geophysical studies conducted over the Laccadive Ridge, northern segment (north of 8°N) of the CLR, suggested the Laccadive Ridge to be of continental origin (Chaubey et al., 2008; Nair et al., 2013) through the delineation of seaward dipping reflectors (Ajay et al., 2010) and was part of the Western Dharwar craton bounded by the Chapporo lineament and Bhavani shear respectively to the north and south (Nair et al., 2013). Nair et al. (2013) also inferred that the volcanic material seen on the Laccadive Ridge are emplaced as intrusives along pre-existing faults as the Indian plate along with Laccadive Ridge moved over the Reunion hotspot. Recently, based on the U-Pb dating of zircons obtained from basaltic beach sands and trachytic rocks and crustal thickness estimation from the inversion of gravity data, Mauritius and Mascarene Plateau was postulated to overlie a concealed Precambrian microcontinent named Mauritia which included Saya de Malha, Chagos, Cargados-Carajos Banks, Laccadives, Nazreth Bank etc. (Torsvik et al., 2013; Ashwal et al., 2017). Receiver function analysis over the Mauritius islands has provided Moho depths of 21 km (Fontaine et al., 2015) and crustal thickness of 10–15 km (Singh et al., 2016) and suggested that oceanic crust thickened by Reunion plume induced magmatic underplating underlies the Mauritius islands rather than continental crust. The crustal thickness and the Moho depth obtained from the present study over the GMR matches well with that obtained through other geophysical studies over Maldive Ridge as well as over Mauritius and Mascarene Plateau. It is to be noted that magnetic lineations were not observed along the Maldive Ridge (Avraham and Bunce, 1977). The Saya de Malha, Nazareth and the Cargados-Carajos Bank, at an average water depth of 50 m has carbonate sequence followed by basaltic flow (Duncan and Hargraves, 1990) which is very similar to the Maldives Ridge. Basalts recovered from the wells drilled over the Maldive Ridge (ODP site 715) and Mascarene Plateau (ODP sites 706), has given ages decreasing from 57.5 Ma over the Maldives to around 20 Ma over the Mauritius islands. Thus, there exists similarity in characteristics like crustal thickness, Moho depth, carbonate build up, shear wave velocity etc among the Maldive Ridge and other ridges like Mauritius, Saya de Malha, etc., which has been interpreted as either to overlay a Precambrian microcontinent or oceanic crust with thick underplating. A thick crust, like the one obtained in the present study is expected in either case ie., if the ridge is underlain by thick magmatic underplating or continental crust. Each of the studies carried to understand the nature of these ridges have their own potential and drawback. Hence more studies with better resolution data is required to firmly ascertain the nature of these ridges which has to be finally confirmed through drilling and has to fit in the plate reconstruction models.

6. Conclusions

Crustal thickness and Moho depth variation over Maldive Ridge and adjoining areas is computed through the inversion of Complete Bouguer Gravity Anomalies (CBA) and Mantle Residual Gravity Anomalies (MRGA). The Moho depth computed using Mantle Residual Gravity Anomalies, incorporating lithospheric thermal and pressure correction has considerable improvement in oceanic areas. However, along the Greater Maldive Ridge (Maldive Ridge, channel between Maldive Ridge and Chagos Bank, northern limit of Chagos Bank), there was not much variation in the computed Moho depth with and without the thermal and pressure gravity corrections suggesting that the crustal thickness of the ridge does not depend on the oceanic isochrones used for the thermal corrections. The predicted Moho depths in the study region ranges from 7 km to 28 km and the thickest crust and the deepest Moho is found below the N-S trending GMR of the Chagos-Laccadive Ridge. The average Moho depths computed for Arabain Basin (∼8.8 km) matched well with the depths obtained from the available seismic refraction stations. The Central Indian Basin, in the study region can be divided into a northern and southern segment. While the southern segment (south of 0°N) is purely oceanic crust with no evidence of magmatic underplating, the thicker crust in northern segment may be explained as either due to magmatic underplating of oceanic crust or a reworked stretched continental crust. Over the Greater Maldive Ridge, a thicker crust and deeper Moho is obtained, with both the crustal thickness and Moho depths decreasing from north to south. The thick crust over the Maldive Ridge (average 22 km) can be explained as either due to magmatic underplating from the Reunion plume or a continental crust; much of the previous geophysical studies supporting thick crust as due to magmatic underplating. Even though there are similarities between Maldive Ridge and other regions like Mascarene Plateau which was recently interpreted as underlain by continental crust, much more geoscientific work including drilling has to be undertaken to finally confirm the exact nature of the Maldive Ridge.

Acknowledgement

The authors thank the Director, Indian Institute of Geomagnetism, Mumbai, for his constant encouragement and support and according permission to publish this work. We earnestly thank reviewers Dr. Yatheesh V., an Anonymous reviewer and the Editor for their meticulous reviews and constructive criticisms, which have greatly improved the paper. Funds for carrying out this research at the Indian Institute of Geomagnetism is provided by the Department of Science and Technology (DST), Government of India, New Delhi, India. Figs. 9 and 10 are generated using GMT Software (Wessel and Luis, 2017).

References

Ajay, K.K., Chaubey, A.K., Krishna, K.S., Gopala Rao, D., Sar, D., 2010. Seaward dipping reflectors along the SW continental margin of India: evidence for volcanic passive margin. J. Earth Syst. Sci. 119, 803–813.

Ashalatha, B., Subrahmanyam, C., Singh, R.N., 1991. Origin and compensation of Chagos-Laccadive Ridge, Indian ocean, from admittance analysis of gravity and bathymetry data. Earth Planet. Sci. Lett. 105, 47–54.

Ashwal, L.D., Wiedenbeck, M., Torsvik, T.H., 2017. Archaean zircons in Miocene oceanic hotspot rocks establish ancient continental crust beneath Mauritius. Nat. Commun. 8, 1–9.

Avraham, B.Z., Bunce, E.T., 1977. Geophysical study of the Chagos-Laccadive Ridge, Indian Ocean. J. Geophys. Res. 82, 1295–1305.

Backman, J., Duncan, R.A., et al., 1988. Proc. ODP, Init. Repts., 115. Ocean Drilling Program, College Station, TX, pp. 589–656.

Bai, Y., Williams, S.E., Müller, R.D., Liu, Z., Hosseinpour, M., 2014. Mapping crustal thickness using marine gravity data: methods and uncertainties. Geophysics 79, G27–G36.

Barthelmes, F., Köhler, W., 2016. International Centre for Global Earth Models (ICGEM), in: Drewes, H., Kuglitsch, F., Adám, J. et al. (Eds.), The Geodesists Handbook 2016, J. Geodesy. vol. 90, pp. 907–1205.

Bhattacharya, G.C., Chaubey, A.K., 2001. Western Indian Ocean – a glimpse of the tectonic scenario. In: Sen Gupta, R., Desa, E. (Eds.), The Indian Ocean – A Perspective. Oxford-IBH, New Delhi, pp. 691–729.

Blakely, R.J., 1995. Potential Theory in Gravity and Magnetic Applications. Cambridge University Press.

Cande, S.C., Patriat, P., 2015. The anticorrelated velocities of Africa and India in the Late Cretaceous and early Cenozoic. Geophys. J. Int. 200, 227–243.

Chappell, A.R., Kusznir, N.J., 2008. Three-dimensional gravity inversion for Moho depth at rifted continental margins incorporating a lithosphere thermal gravity anomaly correction. Geophys. J. Int. 174, 1–13.

Chaubey, A.K., Bhattacharya, G.C., Murty, G.P.S., Srinivas, K., Ramprasad, T., Rao, D.G., 1998. Early Tertiary seafloor spreading magnetic anomalies and paleo-propagators in the northern Arabian Sea. Earth Planet. Sci. Lett. 154, 41–52.

Chaubey, A.K., Srinivas, K., Ashalatha, B., Rao, D.G., 2008. Isostatic response of the Laccadive Ridge from admittance analysis of gravity and bathymetry data. J. Geodyn. 46, 10–20.

Cowie, L., Kusznir, N., 2012. Mapping crustal thickness and oceanic lithosphere distribution in the Eastern Mediterranean using gravity inversion. Pet. Geosci. 18, 373–380.

Davis, W.M., 1928. The coral reef problem, Spec. Publ. 9. Amer. Geogr. Soc., New York, pp. 524–534.

Dietz, R.S., Holden, J.C., 1970. Reconstruction of Pangaea: Breakup and dispersion of continents, Permian to Present. J. Geophys. Res. 75, 4939–4956.

Divins, D.L., 2003. Total Sediment Thickness of the World's Oceans & Marginal Seas. NOAA National Geophysical Data Center, Boulder, Colorado, USA.

Duncan, R.A., R.B. Hargraves, 1990. In: Duncan, R.A., Backman, J., Peterson, L.C. et al. (Eds.), Proceedings of the Ocean Drilling Program, College Station, Texas, Scientific Results, vol. 115, pp. 43–51.

Fisher, R.L., Sclater, J.G., McKenzie, D.P., 1971. Evolution of the Central Indian Ridge, Western Indian Ocean. Geol. Soc. Am. Bull. 82, 553–562.

Fisk, M.R., Howard, K.J., 1990. Primary mineralogy of Leg 115 basalts. In: Duncan, R.A., Backman, J., Peterson, L.C., et al. (Eds.), Proc. ODP, Sci. Results, 115. Ocean Drilling Program, College Station, TX, pp. 23–51.

Fontaine, F.R., Barruol, G., Tkalčić, H., Wölbern, I., Rümpker, G., Bodin, T., Haugmard, M., 2015. Crustal and uppermost mantle structure variation beneath La Réunion hotspot track. Geophys. J. Int. 203, 107–126.

Förste, C., Bruinsma, S., Abrikosov, O., Lemoine, J.M., Marty, J.C., Flechtner, F., Balmino, G., Barthelmes, F., Biancale, R., 2015. EIGEN-6C4, The latest combined global gravity field model including GOCE data up to degree and order 2190 of GFZ Potsdam and GRGS Toulouse. GFZ Data Services.

Francis, T.J.G., Shor, G.G., 1966. Seismic refraction measurements in the northwest Indian Ocean. J. Geophys. Res. 71, 427–449.

Fullea, J., Fernàndez, M., Zeyen, H., 2008. FA2BOUG-A FORTRAN 90 code to compute Bouguer gravity anomalies from gridded free-air anomalies: Application to the Atlantic-Mediterranean transition zone. Comput. Geosci. 34, 1665–1681.

Geosoft, 2014. Oasis montage data processing and analysis (DPA) systems for Earth Science Applications (ver.8.0). GM-SYS version 7.0 Gravity and magnetic modeling software user guide. Geosoft Inc, Canada.

Gómez-Ortiz, D., Agarwal, B.N.P., 2005. 3DINVER.M: A MATLAB program to invert the gravity anomaly over a 3D horizontal density interface by Parker-Oldenburg's algorithm. Comput. Geosci. 31, 513–520.

Greenhalgh, E.E., Kusznir, N.J., 2007. Evidence for thin oceanic crust on the extinct Aegir Ridge, Norwegian Basin, NE Atlantic derived from satellite gravity inversion. Geophys. Res. Lett. 34, L06305.

Gupta, S., Mishra, S., Rai, S.S., 2010. Magmatic underplating of crust beneath the Laccadive Island, NW Indian Ocean. Geophys. J. Int. 183, 536–542.

Henstock, T.J., Thompson, P.J., 2004. Self-consistent modelling of crustal thickness at Chagos-Laccadive ridge from bathymetry and gravity data. Earth Planet. Sci. Lett. 224, 325–336.

Kahle, H.G., Chapman, M., Talwani, M., 1978. Detailed 1×1 gravimetric Indian Ocean Geoid and comparison with Geos-3 radar altimeter geoid profiles. Geophys. J. R. Astron. Soc. 55, 703–720.

Kalra, R., Srinivasa Rao, G., Fainstein, R., Radhakrishna, M., Bastia, R., Chandrashekar, S., 2014. Crustal architecture and tectono-magmatic history of the western offshore of India: Implications on deepwater sub-basalt hydrocarbon exploration. J. Pet. Sci. Eng. 122, 149–158.

Krishnan, M. S., 1960. Geology of India and Burma, fourth ed., vol. 604. Higginbohams, Madras.

Kroll, H., Kirfel, A., Heinemann, R., Barbier, B., 2012. Volume thermal expansion and related thermophysical parameters in the Mg, Fe olivine solid-solution series. Eur. J. Mineral. 24, 935–956.

Laske, G., Masters, G., Ma, Z., Pasyanos, M., 2013. Update on CRUST1.0 – A 1-degree Global Model of Earth's Crust. In: EGU General Assembly Conference Abstracts 15, p. 2658.

Leahy, G.M., Collins, J.A., Wolfe, C.J., Laske, G., Solomon, S.C., 2010. Underplating of the Hawaiian Swell: evidence from teleseismic receiver functions. Geophys. J. Int. 183, 313–329.

Li, C.F., Wang, J., 2016. Variations in Moho and Curie depths and heat flow in Eastern and Southeastern Asia. Mar. Geophys. Res. 37, 1–20.

Lowrie, W., 2007. Fundamentals of Geophysics, second ed. Cambridge University Press (ISBN-13 978-0-521-67596-3).

Ma, Z., Dalton, C.A., 2017. Evolution of the lithosphere in the Indian Ocean from combined earthquake and ambient noise tomography. J. Geophys. Res. Solid Earth 122, 354–371.

McKenzie, D.P., 1978. Some remarks on the development of sedimentary basins. Earth Planet. Sci. Lett. 40, 25–32.

McKenzie, D., Jackson, J., Priestley, K., 2005. Thermal structure of oceanic and continental lithosphere. Earth Planet. Sci. Lett. 233, 337–349.

McKenzie, D., Sclater, J.G., 1971. The evolution of the Indian Ocean since the Late Cretaceous. Geophys. J. R. Astron. Soc. 25, 437–528.

Morgan, W.J., 1972. Deep mantle convection plumes and plate motions. Am. Assoc. Pet. Geol. Bull. 56, 203–213.

Morgan, W.J., 1981. In: Emiliani, C. (Ed.), The Sea (Vol. 7): The Oceanic Lithosphere. Wiley-Interscience, NewYork, pp. 443–487.

Mukhopadhyay, R., Ghosh, A.K., Iyer, S.D., 2008. The Indian Ocean Nodule Field: Geology and Resource Potential, Handbook of Exploration and Environmental Geochemistry.

Müller, R.D., Royer, J.-Y., Lawver, L.A., 1993. Revised plate motions relative to the hotspots from combined Atlantic and Indian Ocean hotspot tracks. Geology 21, 275–278.

Müller, R.D., Sdrolias, M., Gaina, C., Roest, W.R., 2008. Age, spreading rates, and spreading asymmetry of the world's ocean crust. Geochem. Geophys. Geosyst. 9, Q04006.

Naini, B.R., M. Talwani, 1983. In: Watkins, S., Drake, C.L. (Eds.), Studies in Continental Margin Geology, American Association Petroleum Geologists Memoir 34, Tulsa, Oklahoma, pp. 167–191.

Nair, N., Anand, S.P., Rajaram, M., 2013. Tectonic framework of Laccadive Ridge in Western Continental Margin of India. Mar. Geol. 346, 79–90.

Narain, Hari, Kaila, K.L., Verma, R.K., 1968. Continental margins of India. Can. J. Earth Sci. 5, 1051–1065.

Nathaniel, D.M., D'Silva, K., Muralikrishna, A., Chandra Rao, D., 2011. Synergy of concepts and technology redefines the WCMI and enhances petroleum exploration opportunities. In: Proceedings of the 7th International Conference on Asian Marine Geology, 11–14 October.

Oldenburg, D.W., 1974. The inversion and interpretation of gravity anomalies. Geophysics 34, 526–536.

Parker, R.L., 1972. The rapid calculation of potential anomalies. Geophys. J. R. Astron. Soc. 31, 447–455.

Parsons, B., Sclater, J.G., 1977. An analysis of the variation of ocean floor bathymetry and heat flow with age. J. Geophys. Res. 82, 803–827.

Pushcharovsky, Yu.M., 1996. Tectonics of the Indian Ocean. Geotectonics 29, 336–354.

Radhakrishna, T., Joseph, M., 2012. Geochemistry and paleomagnetism of Late Cretaceous mafic dikes in Kerala, southwest coast of India in relation to large igneous provinces and mantle plumes in the Indian Ocean region. GSA Bulletin 124, 240–255.

Sandwell, D.T., Müller, R.D., Smith, W.H.F., Garcia, E., Francis, R., 2014. New global marine gravity model from CryoSat-2 and Jason-1 reveals buried tectonic structure. Science 346, 65–67.

Sandwell, D.T., Smith, W.H.F., 2009. Global marine gravity from retracked Geosat and ERS-1 altimetry: ridge segmentation versus spreading rate. J. Geophys. Res. 114, B01411.

Sawyer, D.S., 1985. Total tectonic subsidence: a parameter for distinguishing crust type at the U.S. Atlantic Continental Margin. J. Geophys. Res. Solid Earth 90, 7751–7769.

Sclater, J.G., Fisher, R.C., 1974. Evolution of the east central Indian Ocean, with emphasis on the tectonic setting of the Ninetyeast Ridge. Bull. Geol. Soc. Amer. 85, 683–702.

Singh, M., Kaviani, A., Rümpker, G., 2016. The crustal structure beneath Mauritius from teleseismic P-receiver functions – oceanic or continental? Geophys. Res. Lett. 43, 9636–9643.

Smith, R.A., 1961. A uniqueness theorem concerning gravity fields. Math. Proc. Cambridge Philos. Soc. 57, 865.

Smith, W.H., Sandwell, D., 1997. Global sea floor topography from satellite altimetry and ship depth soundings. Science 277, 1956–1962.

Stein, C., Stein, S., 1992. A model for the global variation in oceanic depth and heat flow with lithospheric age. Nature 359, 123–128.

Tiwari, V.M., Grevemeyer, I., Singh, B., Morgan, J.P., 2007. Variation of effective elastic thickness and melt production along the Deccan-Reunion hotspot track. Earth Planet. Sci. Lett. 264, 9–21.

Torsvik, T.H., Amundsen, H., Hartz, E.H., Corfu, F., Kusznir, N., Gaina, C., Doubrovine, P.V., Steinberger, B., Ashwal, L.D., Jamtveit, B., 2013. A Precambrian microcontinent in the Indian Ocean. Nat. Geosci. 6, 1–5.

Torsvik, T.H., Tucker, R.D., Ashwal, L.D., Carter, L.M., Jamtveit, B., Vidyadharan, K.T.,

Venkataramana, P., 2000. Late Cretaceous India-Madagascar fit and timing of break-up related magmatism. Terra Nova 12, 220–224.
Wessel, P., Luis, J.F., 2017. The GMT/MATLAB Toolbox. Geochem. Geophys. Geosyst. 18.
White, R.S., McKenzie, D., Onions, K., 1992. Oceanic Crustal Thickness From Seismic Measurements and Rare Earth Element Inversions. J. Geophys. Res. 97, 19683–19715.
Whitmarsh, R.B., 1974. Some aspects of plate tectonics in the Arabian Sea. In: Initial Reports of the Deep Sea Drilling Project, 23. US Govt. Printing Office, Washington, pp. 527–535.
Whittaker, J.M., Goncharov, A., Williams, S.E., Müller, R.D., Leitchenkov, G., 2013. Global sediment thickness data set updated for the Australian-Antarctic Southern Ocean. Geochem. Geophys. Geosyst. 14, 3297–3305.